Extended Abstracts of the 2020 International Conference on Solid State Devices and Materials, VIRTUAL conference, 2020, pp35-36

On-Wafer Electron Beam Detectors by Floating-Gate FinFET Technologies

Chih-An Yang[1], Shi Jiun Wang[1], Burn Jeng Lin[2], Chrong Jung Lin[1], and Ya-Chin King[1]
[1]Institute of Electronics Engineering, National Tsing Hua University, Hsinchu, Taiwan
[2]Institute of Photonics Technologies, National Tsing Hua University, Hsinchu, Taiwan
Phone/Fax: +886-3-5162219, E-mail: ycking@ee.nthu.edu.tw

Abstract

A floating-gate based electron beam (eBeam) detector using lateral contact coupling structure is proposed and realized by advanced CMOS FinFET processes. The negative voltages caused by the charging of the on-wafer sensing pads by eBeam has been demonstrated, leading to change in the corresponding floating gate charge. This detector/recorder has been developed for monitoring on-chip eBeam level without external power source.

Introduction

In modern semiconductor processes, lithographical processes play key roles for enabling the critical dimensions on integrated circuit to be push into nano-meter regime, in which energy sources such as DUV/ EUV and eBeam become inevitable. To obtain feedback on the eBeam intensities on the projected plane, conventional sensors, i.e., Charge-coupled devices (CCD) [1] and Active Pixel Sensor (APS) [2], utilizing potential wells and/or floating nodes for collecting photo-electrons induced by photoelectric effects, are commonly used. In these sensor arrays, each pixel generally composed of a photodiode and multiple transistors. To ensure the integrity of the signal, special channels [3] for charge transferring are required. Therefore, these photo-sensing are realized by specialized processes. On the other hand, high optical resolutions, high energy eBeam is found to penetrate deep into the sensing plan, leading to severe dispersion effects of the injected beams [4]. In this work, a floating gate (FG) based FinFET detector with a stacked energy sensing pad, is designed for enhancing the sensitives as well as the maintaining a good spatial resolution.

Operation Principle and Test Pattern Design

A 3D schematic of the proposed on-wafer eBeam detector with a surface energy sensing pad connected to the slot contacts landed on the STI region as the main coupling structure to the FG is illustrated in **figure 1(a)**. The detector is designed with sensing gate coupling ratio (α_{SG}) of *33%*, while the read gate coupling ratio (α_{RG}) is close to *8%*. In its neutral state, the expected V_{TH} is around *5V*, when accessed from the read-gate. As eBeam charges up the energy sensing pad on the wafer surface, negative sensing pad voltage, V_{SP}, is coupled to FG, pushing electrons out of the FG, as illustrated in **figure 1(b)**. The capacitance level of the sensing pad, C_{SP}, affects how fast V_{SP} raises during eBeam exposure. Measured V_{SP} responses to a test I_{SP} current are arranged in **figure 2**, where C_{SP} of *80fF* is found, a comparable level of a typical probing pad. The I_D-V_{RG} curves in **figure 3** indicates negative V_{TH} shift from its neutral state with increasing eBeam exposure time with an intensity of $1\mu C/cm^2 \cdot sec$ for low energy eBeam of *5keV*. Accumulated charging effect can be found on the recorders, as revealed by data.

Experimental Results and Discussion

The V_{TH} shift response under different flux levels is compared in **figure 4**. To reach $1\mu C/cm^2$ dose, the scan time on the sensing pads is *26, 13, 8.7 sec*, respectively, for eBeam current, I_{eB}, settings of *1, 2, 3pA*. Same V_{TH} shift is obtained for the same electron doses under flux levels of $6x10^{12}$, $12\ x10^{12}$ and $18\ x10^{12}/cm^2 \cdot sec$. The charge stored in floating gate, Q_{FG}, saturates after total dosage reaches $10\mu C/cm^2$. In **figure 5**, the detector's response with increasing scan time is matched by the results obtained by applying different I_{SP} current. Not all injected electrons are collected by the sensing pad, hence, matching I_{SP} found to be lower than that projected by I_{eB}. **Figure 6** compares the detector's responses when electron beam of different energy. As energy increases, the projection range deepened. With a stacked sensing pad, the V_{TH} responses start to reduce when energy exceed *30keV*. **Figure 7** compares the extracted electron collection efficiency on the sensing pads, η, with that obtained by CASINO simulation [5]. As expected, η decreases as electrons inject deeper under the surface. **Figure 8** shows the data retention characteristics, the stored charges inside floating gate (Q_{FG}) remains stable after eBeam exposure, while detectors with Q_{FG} close to the saturated level sees some charge-gain effect. **Figure 9** shows the degradation of sub-threshold swing of detector after high energy beam exposure. This is believed to be caused by the change in the coupling capacitance, which can be problematic for high energy beam sensing. In **figure 10**, the simulated electron distributions of beams with *25keV* and *80keV* is compared. Based on the stacked sensing pads composed of M1to M9, $\eta < 2.8\%$ when accelerating energy reaches *80keV*. To avoid sub-threshold swing degradation and increase electron collection efficiency, an ultra-thick metal (UTM) layer is proposed to extend the sensing pad upward. The simulated electron distributions for a detector with different thickness of UTM are arranged in **figure 11**. The percentage of electrons reach the Si substrate in **figure 12**, revealing that a UTM of a least $12\mu m$ is needed to effectively shield the detector from disturbance for *50keV* beams.

Conclusion

A floating gate eBeam detector has been successfully demonstrated by FinFET technologies. The power-free and on-wafer eBeam detector/ recorder can be used off-line feedback in advanced lithographical systems.

Acknowledgements

The authors would like to acknowledge the support from Taiwan Semiconductor Manufacturing Company and Ministry of Science and Technology, Taiwan (Project Number: MOST 108-2622-8-007-017).

References

[1] W. S. Boyle, et al., in BSTJ, pp. 587-593, 1970.
[2] A. Dickinson, et al., in ARVLSI, pp. 214-224, 1995.
[3] K. Hatano, et al., in IEDM, pp. 903-906, 1996.
[4] E. Munro, et al., in IVELEC, pp. 483-484, 2010.
[5] P. Wu, et al., in ICSICT, pp. 1-3, 2012.

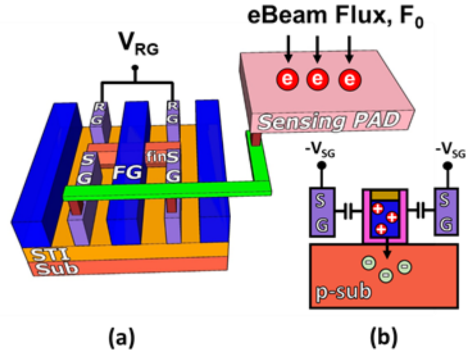

Figure 1. (a) 3D schematic of on-wafer eBeam detector with a surface energy sensing pad. (b)Illustration of how it records during beam exposure.

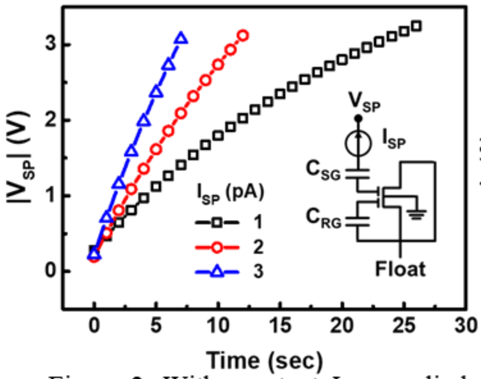

Figure 2. With constant I_{SP} applied, measured V_{SP} response give a sensing pad capacitance of approx. *80fF*.

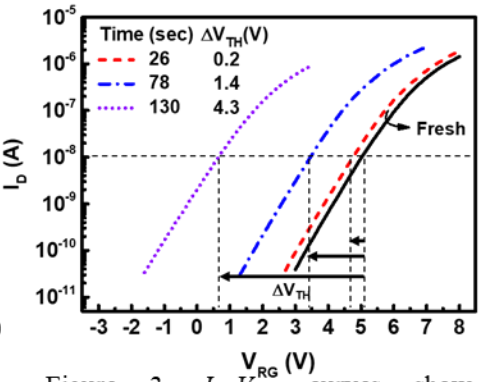

Figure 3. I_D-V_{RG} curves show negative V_{TH} shift after increasing exposure time with an intensity of $1\mu C/cm^2\cdot sec$ under *5keV* energy.

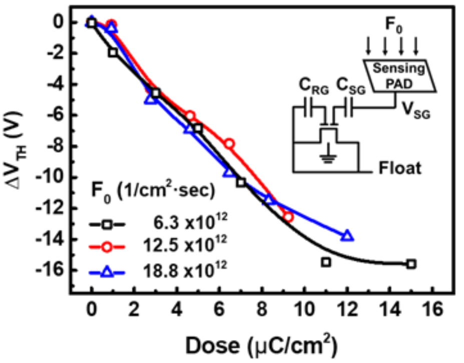

Figure 4. V_{TH} shift responded consistently to the total electron dose injected onto the sensing pad, under different flux intensities.

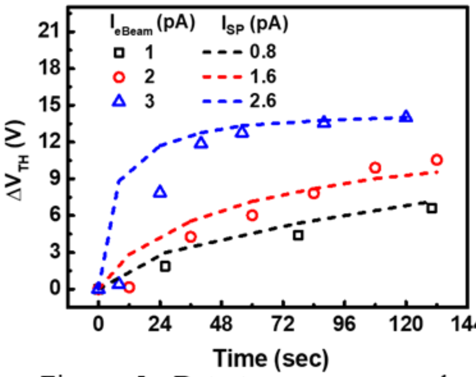

Figure 5. Detector response under eBeam and that by applying equivalent level of current, I_{SP}, on the sensing pad, to obtain the matching responses

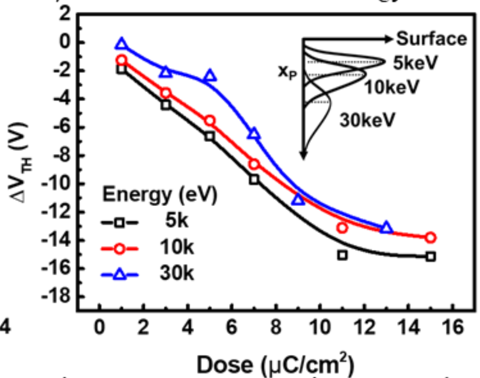

Figure 6. As energy increases, the projected range deepened. With a stacked sensing pad, the response starts to decrease as energy *>30keV*.

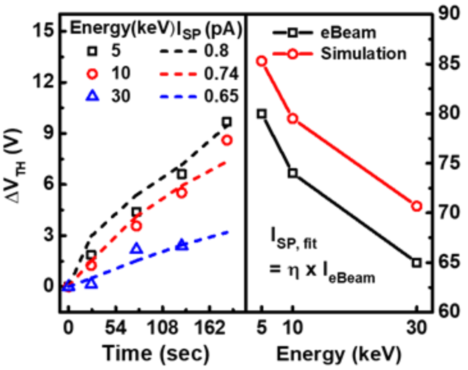

Figure 7. Higher energy beam penetrates deeper under the surface, the e⁻ collection efficiency, η, decreases. Measured η is slightly lower than that extracted from experiments.

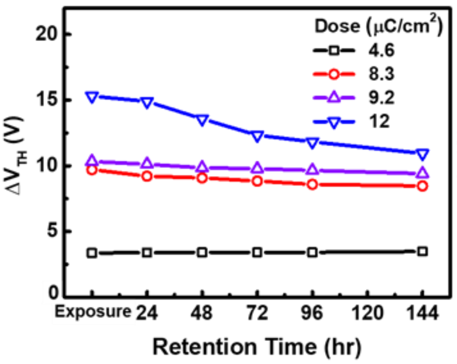

Figure 8. Q_{FG} inside the floating gate remain relative stable after *6 days*. While samples with higher Q_{FG} subject to some charge gain effect.

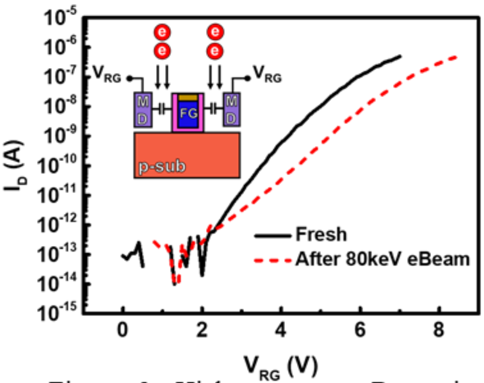

Figure 9. Higher energy eBeam is found to cause a range in the sub-threshold swing of the detectors, with lowered coupling ratio.

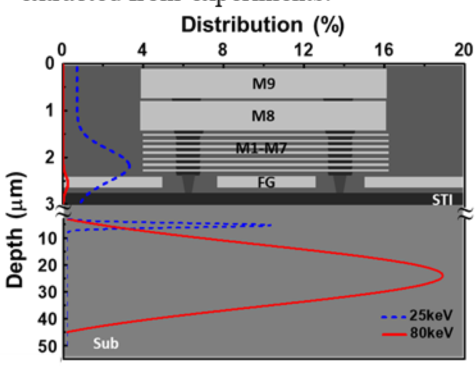

Figure 10. Simulated projection ranges for eBeam at different energy, as compare to the chip's metal layers

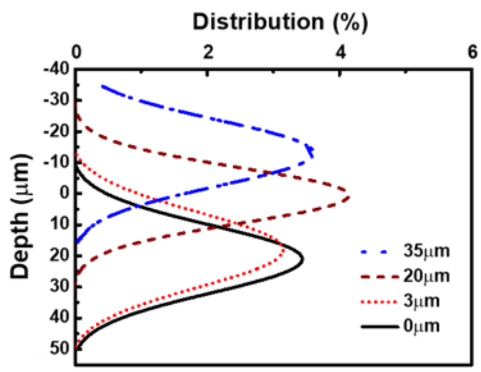

Figure 11. The peak of electron distributions in depth depend on the design of UTM, to avoid electron injection onto Si substrate.

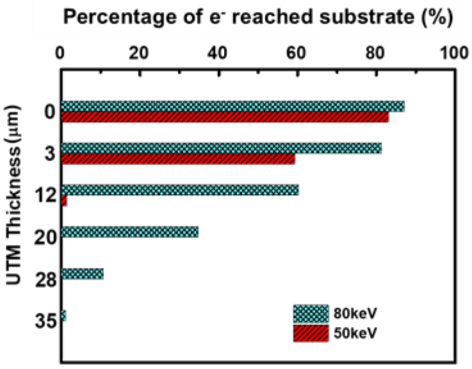

Figure 12. Portion of electron penetrating to Si substrate in under different UTM thicknesses design.